Research paper

A fiber reinforced poroelastic model of nanoindentation of porcine costal cartilage: A combined experimental and finite element approach

Shikha Gupta[a], Jeremy Lin[b], Paul Ashby[c], Lisa Pruitt[e,d,*]

[a] Medical Polymers and Biomaterials Group, Department of Applied Science and Technology, University of California, Berkeley, CA, 94720, USA
[b] Department of Restorative Dentistry, University of California, San Francisco, CA, 94143, USA
[c] Imaging and Manipulation of Nanostructures Facility, Molecular Foundry, Lawrence Berkeley National Labs, Berkeley, CA 94720, USA
[d] Department of Orthopaedic Surgery, University of California, San Francisco, CA, 94110, USA
[e] Department of Mechanical Engineering, University of California, Berkeley, CA, 97420, USA

ABSTRACT

Nanoindentation has shown promise as a mechanical characterization tool for orthopaedic biomaterials since it can probe the properties of small, heterogeneous, irregularly shaped tissue volumes in physiological environments. However, the majority of nanoindentation analyses have been limited to the determination of linear elastic and viscoelastic properties. Since biomaterials possess complex nonlinear, hydrated, time-dependent constitutive behavior, the objective of the present study is to explore the ability of nanoindentation to determine physiologically relevant material properties using a fibril reinforced poroelastic (FRPE) model. A further goal is to ascertain the sensitivity of nanoindentation load–displacement curves to different FRPE parameters, including the elastic properties of the nonfibrillar matrix, the composition and distribution of fibers, and nonlinearity in the fluid permeability. Porcine costal cartilage specimens are experimentally tested with nanoindentation load relaxation experiments at two different loading depths and loading rates. The FRPE material properties are extracted from comparisons to finite element simulations. The study demonstrates the behavior of the model in nanoindentation is distinct from bulk indentation; the static response of the nanoindentation is determined almost exclusively by the elastic properties of the nonfibrillar matrix and the volume fraction of fibers, while the transient response is dominated by the fluid permeability of the tissue. The FRPE model can accurately describe the time-dependent mechanical behavior of costal cartilage in nanoindentation, with good agreement between experimental and numerical curve fits ($R^2 = 0.98 \pm 0.01$) at multiple indentation depths and indentation rates.

© 2009 Published by Elsevier Ltd

* Corresponding address: Medical Polymers and Biomaterials Laboratory, University of California, Berkeley, 5134 Etcheverry Hall, Berkeley, CA, 94720, USA. Tel.: +1 510 642 2595; fax: +1 510 643 5599.
E-mail address: lpruitt@me.berkeley.edu (L. Pruitt).

1. Introduction

The use of small animal models in orthopaedics research, such as rat and rabbit models, has accelerated the rate at which disease progression, repair and regeneration in orthopaedic tissues can be explored. Like their healthy counterparts, diseased tissues and repair tissues found in small animal models are complex; they exhibit transient behaviors associated with extracellular matrix viscoelasticity and fluid flow, they have complex microstructures with several regions of distinct composition and hierarchical structure, and they are present only in very small volumes. These attributes still permit the spatiotemporal biochemical characterization of the tissues using histology and immunohistochemisty, but they preclude the use of global mechanical testing protocols for characterizing their heterogeneous mechanical properties. Since orthopaedic tissues are load-bearing materials, characterization of biochemical properties alone is not sufficient for assessing the health and functionality of the tissues — a fundamental understanding of the mechanical properties is also requisite.

The advent of nanoindentation instruments has provided a method for determining time-dependent mechanical properties on a size scale compatible with tissue dimensions in controlled, physiological environments (Haque, 2003; Ebenstein and Pruitt, 2006). Unlike bulk indentation, typical nanoindentation loads and displacements are on the order of hundreds of nanonewtons and hundreds of nanometers, respectively, making the technique suitable for testing sub-millimeter tissues volumes.

Current nanoindentation tools were developed to characterize hard, isotropic elasto–plastic thin films (Bhushan et al., 1988; Pharr and Oliver, 1992). As such, widely used analytical methods for determining material properties from nanoindentation load displacement curves, such as the Oliver–Pharr method, are derived from Hertz contact theory and assume that the material of interest is a smooth (flat), homogeneous, isotropic, elastic–plastic half-space (Sneddon, 1965; Doerner and Nix, 1986; Oliver and Pharr, 1992). The constitutive behavior of mineralized biomaterials is in many ways comparable to that of traditional elastic–plastic materials. Though mineralized tissue samples are usually dehydrated before testing, the standard nanoindentation technique has been used successfully over the past decade to study the hardness and elastic modulus of the tissues such as bone, teeth, and atherosclerotic plaque (Rho et al., 1999; Zysset et al., 1999; Balooch et al., 2004; Ho et al., 2004; Oyen and Ko, 2007; Oyen, 2008). Soft tissues, on the other hand, are hydrated materials with complex constitutive behaviors that violate all the aforementioned analytical assumptions. Limited nanoindentation work has been conducted on soft tissues, including repair cartilage, fibrocartilage, vascular tissue, and the healing fracture callus, with the authors generally reporting elastic properties or functional parameters (Hu et al., 2001; Ebenstein et al., 2004; Ebenstein and Pruitt, 2004; Li et al., 2006; Franke et al., 2007; Li et al., 2007; Leong and Morgan, 2008). This is due in large part to the fact that analytical solutions to the indentation, whether macroscale, microscale, or nanoscale, are very limited, existing only for select tip geometries, loading profiles, and simple material models including linear elastic, linear viscoelastic models, and in the case of porous, free-draining flatpunch indentation, linear poroelastic materials (Hertz, 1881; Sneddon, 1965; Mak et al., 1987; Sakai, 2002; Mattice et al., 2006; Oyen, 2006). So while nanoindentation, unlike other mechanical characterization methods, has the experimental benefit of permitting in-situ testing on irregularly shaped specimens, nearly all indentation solutions for complex constitutive models are analytically intractable.

Over the past decade, several investigators have surmounted the challenge by coupling indentation tests with numerical finite element (FE) simulations of indentation. FE analyses have been used extensively with nanoindentation experiments of semiconductor thin films, ceramics, and nanocomposites to determine residual stress in multilayered films, to study pile-up/sink-in, and to assess thin film fracture toughness (Bhattacharya and Nix, 1988; Bolshakov et al., 1996; Weppelmann and Swain, 1996; Bolshakov and Pharr, 1998; Elmustafa, 2007). To date, FEM of orthopaedic soft tissue nanoindentation has been limited primarily to parametric studies of different elastic and linear viscoelastic material models, with a single study on mouse articular cartilage (Gupta et al., 2005; Cao et al., 2006).

However, simulations conducted on macroscale indentation of compliant biomaterials using more physiological constitutive models have been reported by numerous authors. Olberding and Suh (2006) utilized differential evolution algorithms to optimize material parameters for articular cartilage and agarose while Wilson et al. (2004) and Lei and Szeri (2007) coupled experiments with commercial FEM codes using nonlinear optimization tools in MATLAB (DiSilvestro and Suh, 2001; Wilson et al., 2004; Olberding and Suh, 2006; Lei and Szeri, 2007). These studies have utilized several sophisticated biphasic constitutive models which have evolved over the last three decades. The simplest biphasic models treat the material as a binary mixture of an immiscible solid and fluid phase, both of which are considered incompressible. The constitutive response of these materials is governed both by the deformation of the solid constituents, pressurization of the fluid, and the viscous drag due to solid–fluid interactions.

In recent years, fibril reinforced poroviscoelastic (FRPE) models have emerged as the most applicable models for describing the mechanical behavior of orthopaedic soft tissues under many different testing modes, including uniaxial tension, unconfined compression, confined compression and indentation (Li et al., 2000; Wilson et al., 2004; Li and Herzog, 2004a; Li et al., 2005). In FRPE models, the solid phase is composed of two distinct constituents — a semi-solid gel and a fibrous network. Li et al. (2001) and Korhonen et al. (2003) have used FRPE models to simulate the unconfined compression response of both healthy and osteoarthritic articular cartilage (Li et al., 2001; Korhonen et al., 2003). More recent studies have extended the model to include the intrinsic viscoelasticity of the fiber response and matrix deformation due to osmotic forces (Li and Herzog, 2004a; Wilson et al., 2005).

The success of these studies suggests that FRPE models should be effective in characterizing the nanoindentation response of orthopaedic soft tissues. However, further experimental testing and numerical validation is still required. Nanoindentation experiments, due to the small volumes of test material, are more sensitive than bulk

indentation to local material heterogeneity, to surface adhesion, and surface roughness — factors which may have to be accounted for in both theoretical and numerical analyses (Carrillo et al., 2005). In addition, unlike most continuum models, fibril reinforced poroelastic models are sensitive to the tissue dimensions and experimental length scales so that results from bulk experiments may not translate directly to nanoindentation *a-priori*. Thus, the objective of the present study is to explore the response of fibril reinforced poroelastic models in nanoindentation and to determine whether these models can effectively predict the properties of porcine costal cartilage from nanoindentation experiments.

2. Materials and methods

In the present study, porcine costal cartilage (PCC) specimens were tested experimentally with nanoindentation. PCC was chosen as a test material since, like other types of hyaline cartilage, it is made up of three primary constituents — (i) a solid phase consisting of a collagen II fiber network, (ii) a proteoglycan matrix, and (iii) an ionic fluid phase. It thus exhibits the nonlinear viscoelastic response typical of most soft tissues. In addition, PCC is also a suitable control tissue since it is considered to be uniformly heterogeneous — it is a multiphasic material, but it should have nearly uniform composition with a randomly oriented collagen fiber network over several mm^3 volumes (Mallinger and Stockinger, 1988; Pietila et al., 1999; Feng et al., 2001). Such uniformity facilitates FE analysis since it results in isotropic material behavior at small strains, minimizing the confounding effects of surface and depth dependent anisotropy in the material.

A finite element model of the nanoindentation experiments was constructed using a FRPE model. The finite element simulations were used to study the general behavior of the FRPE model in nanoindentation and its sensitivity to different constituent parameters, and to determine its success in describing the nonlinear nanoindentation response of the PCC.

3. Experimental methods

3.1. Sample preparation

Three young porcine whole spare ribs were obtained from a local abattoir within 24 h of sacrifice. The third and fourth costal ribs were dissected from the sternum of each slab and cut into multiple specimens. From each rib ($n = 5$) one specimen, approximately 3 mm thick, was cored for nanoindentation and snap frozen in optimal cutting temperature solution (OCT). Since nanoindentation depths are less than 5 μm, experimental load–displacement curves are sensitive to surface asperities and roughness. To minimize errors from asperities, the top and bottom surfaces of the PCC specimens were cryomicrotomed prior to testing to ensure a smooth indentation surface. An additional specimen was cut adjacent to the nanoindentation specimen and snap frozen in OCT for further sectioning and histological examination with Safranin-O/Fast Green and Alizarin-Red.
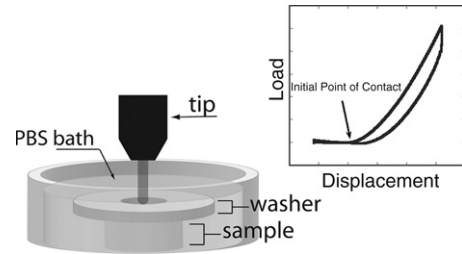

Fig. 1 – Schematic of the experimental setup for nanoindentation of porcine costal cartilage. A 100 μm radius of curvature fluid cell tip is used to test the specimen, which is immersed in a room temperature phosphate buffered saline bath and clamped to prevent it from floating freely in the bath. To accurately determine the total penetration of the tip, all indents start from a few hundred nanometers above the anticipated surface and the initial point of contact is determined visually from individual load–displacement curves.

3.2. Nanoindentation

Frozen samples were first brought to room temperature by thawing in air. The OCT was removed by repeated rinsing with phosphate buffered saline (PBS) for approximately 30 min. During experimentation, all specimens were placed in a Petri dish and immersed in room temperature PBS supplemented with protease inhibitors (5 mM benzamide-HCL and 10 mM N-ethylmaleimide) to prevent autolytic activity during experimentation.

All indents were performed using a Hysitron TriboIndenter (Hysitron, Minneapolis, MN) in displacement controlled feedback mode. Indents were taken with a 100 μm radius of curvature conospherical diamond indenter. To facilitate testing in fluid, the diamond tip was attached to a 5 mm long titanium shaft (Fig. 1). Indents were performed on 11 to 12 different positions on each of the 5 specimens. A trapezoidal displacement profile was applied to the indenter. The indenter displacement was linearly ramped to a maximum penetration depth of either 2.0 μm or 3.1 μm at a displacement rate of either 0.2 μm/s or 2 μm/s, followed by a 150 s hold period at the maximum penetration depth, and withdrawn at a rate of 0.2 μm/s. Typical nanoindenters use a load setpoint (usually 1–2 μN) on the indenter tip to detect the sample surface, and the detection point is assumed be the point of zero tip deformation (penetration). Though an indenter load of 1 μN results in negligible deformation in mineralized tissues, such loads may cause several hundred nanometers of indentation in compliant tissues. Thus, to ensure the accurate measurement of the penetration depth, the nanoindenter tip was withdrawn from the cartilage sample by 1 μm after reaching the load set-point, and all indents were initiated with the tip above the surface of the cartilage. For each indentation position, the initial point of contact was determined visually from an initial load–displacement curve (Fig. 1). The total tip displacement (distance between the tip and cartilage surface plus the tip penetration depth into the surface) was then adjusted to achieve the desired maximum penetration depth of 2.0 or 3.1 μm for each indent.

A total of 44–48 indents were performed on each specimen. Four indents were performed sequentially at every position — one indent at each of the two depths and the two loading rates (in randomized order). A three minute recovery period was allowed between each of the four indents. The experiments with longer recovery times were conducted, but three minutes was found to be sufficient for complete recovery of the cartilage, and it resulted in the most reproducible load–displacement curves. For each rib specimen, the experimental load–time data from all 12 indents with the same indentation depth and indentation rate was averaged and compared to finite element simulations.

4. Numerical methods

Since analytical solutions for the indentation of FRPE materials do not exist, numerical finite element simulations had to be be utilized along with the experimental results to determine the fibril reinforced material properties.

4.1. Finite element model

All simulations were performed using ABAQUS Standard v.6.7 (Simulia, Providence, RI). The substrate (cartilage) geometry was constructed in Patran (2005, MSC Software Co., Santa Ana, CA, USA), while the indenter geometry was modeled directly in ABAQUS (Fig. 2(a)). Since the stiffness of the diamond indenter is nearly six orders of magnitude greater than the cartilage substrate, the indenter geometry was modeled as an axisymmetric 2D rigid surface. To ensure an accurate computation of the contact area, the dimension of the substrate surface elements was 1% of the indenter radius. Since friction was found to have a negligible effect on the simulated load–displacement curves, a frictionless, finite sliding contact formulation was used between the indenter and cartilage substrate. Rigid displacement boundary conditions were assumed for the bottom edge of the substrate. Fluid flow was prohibited at the inner radial boundary ($R = 0$) and a zero pore pressure (free-draining) condition was set for the outer radial boundary. An evolving fluid-flow boundary condition was utilized on the top contact surface; all elements started off with free draining fluid flow conditions. As nodes on surface elements came into contact with the indenter, the elements effectively 'sealed', preventing fluid flow in the direction normal to the indenter surface (Warner et al., 2001a,b). Fig. 3(b) shows a symbol plot of the fluid velocity, and depicts the sealing of elements during indentation. During the simulation, the displacement profile applied during the nanoindentation experiments was applied to the rigid indenter.

4.2. Material model

A FRPE model was used in the simulations. While all poroelastic models independently model the contribution of the solid and fluid phases of the tissues to the overall mechanical response, the hallmark of FRPE models is the further breakdown of the solid phase into a distinct fiber network representing the collagen component and a semi-solid gel representing the proteoglycan matrix, both of which are modeled independently in the finite element construction. The nonfibrillar proteoglycan matrix is generally modeled as a permeable, linear elastic, hyperelastic or viscoelastic solid; the collagen fibers are usually modeled as one-dimensional nonlinear elastic or viscoelastic elements that only sustain tension. Viscoelastic effects may be included in the solid phases to model the intrinsic time-dependent response of the tissues, independent of the transient response due to fluid–solid interactions. Fluid flow in the system is described by the permeability, κ, of the nonfibrillar matrix. In the present study, the porous, nonfibrillar proteoglycan matrix was represented with isotropic, linear elastic 2D bilinear pore pressure elements (CAX4P). The pores are saturated with a single fluid with a fixed permeability (κ). A dilation-dependent permeability of the following form can be assumed (Lai and Mow, 1980):

$$\kappa = \kappa_0 \exp\left(M \frac{e - e_0}{1 + e_0} \right) \tag{1}$$

where e is the porosity (void ratio), e_0 is the initial porosity, M is a nonlinearity factor, and κ_0 is the initial permeability, results from a sensitivity analysis (see below) show that the nonlinearity factor M has negligible impact on the nanoindentation load–displacement response. Prior FRPE models have represented fibers as 1D nonlinear spring elements, as 2D membranes elements, and as user-defined embedded elements (Fortin et al., 2000; Wilson et al., 2004; Shirazi and Shirazi-Adl, 2005). In the present model, the fibrillar collagen component was introduced as 1D rebar elements embedded into the nonfibrillar proteoglycan matrix. To model the tension–compression nonlinearity of the collagen fibers and the collapse of the fibers in compression, the individual rebar elements (REBAR) resisted only tensile stresses. In ABAQUS, rebar elements have two geometric properties: orientation angle and cross-sectional area, both of which determine the volume fraction of fibers in the model. The collagen fibers in young porcine costal cartilage are randomly oriented. Since an exact spatial distribution of the fibers was not available, the random fiber distribution was mimicked in the present study through fifteen different fiber orientations. Fibers were oriented parallel to the radial (r), axial (z), and circumferential (θ) directions (0°) and at ±30° and ±60° from the r, z, and θ axes (Fig. 4). The inclusion of fibers at additional orientations was found to have a negligible effect on the numerical L–D response. The fibers were modeled with a fixed nonlinear elastic constitutive response determined from the tensile stress–strain curve of collagen fibers (Morgan, 1960; Haut and Little, 1972). Though viscoelasticity of the fibers was found to play an important role in the macroscopic tensile response of articular cartilage, it was presently ignored, since fiber viscoelasticity has a negligible effect on time-dependent behavior, compared to fluid pressurization when compression is the dominant mode of deformation (Li et al., 2005). Material parameters in the model were thus the Young's modulus (E_m) and Poisson's ratio (v_m) of the nonfibrillar proteoglycan matrix, the fluid permeability (κ) and the volume fraction (f_f) of collagen fibers.
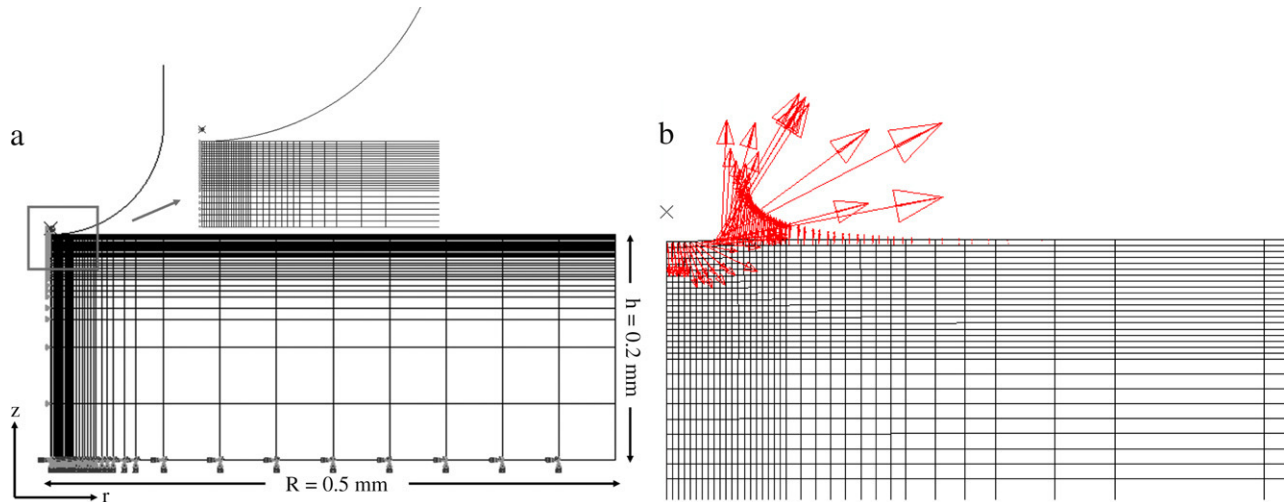
Fig. 2 – (a) The two dimensional axisymmetric finite element model consists of 1550 four node bilinear elements with the finest elements under the anticipated indenter edge. **(b)** A symbol plot of the pore fluid velocity in the elements below the indenter tip during indentation depicting the evolving pore pressure boundary condition. Initially, a free-draining fluid flow condition exists at the cartilage surface. As surface elements come into contact with the indenter, fluid flow in the direction normal to the indenter is sealed.
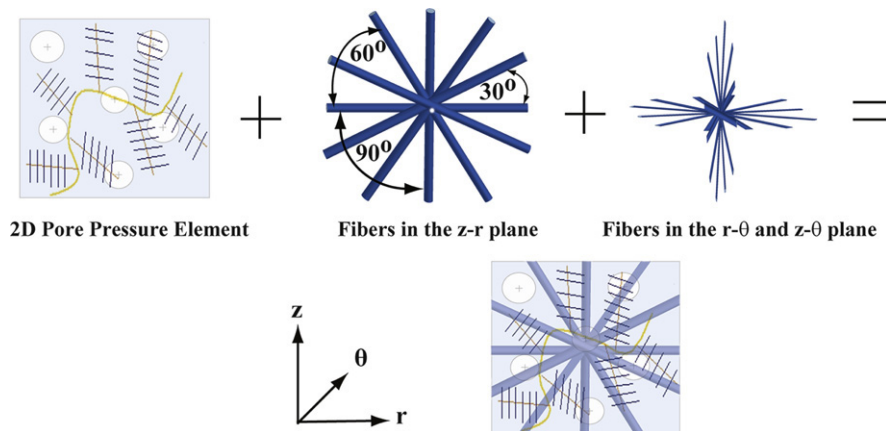

Fig. 3 – The porous, nonfibrillar matrix is represented with 2D pore pressure elements and the randomly distributed collagen fibers are modeled with 1D embedded rebar elements oriented in 15 different directions at 0°, ±30°, and ±60° from the r, z, and θ axes.

4.3. Curve fitting — Interpolant response surface

With any multi-parameter constitutive model, determining the values of the material properties that best fit a particular set of experimental data, requires a suitable curve-fitting method, irrespective of the existence of an analytical solution. Most curve-fitting procedures take an initial guess of material parameters as input to either the analytical or numerical model, and the parameters are updated iteratively using a gradient-based or heuristic optimization scheme until a suitable fit between the experimental data and the model results is achieved. Rather than employing an iterative method, the present study utilized a custom written MATLAB (v. 6.0 MathWorks Inc., 1984–2002) code[1] to generate a multi-dimensional interpolant response surface (IRS) to optimize

the agreement between finite element (FE) simulations and experimental data (Keenan et al., 2007) and find the best fit material parameters for the FRPE model. A general description of an IRS and its construction, which involves several steps, follows:

(i) Selection of a physiologically relevant range for all the material parameters. In the present study, the indenter load, P, was assumed to be a function of five independent variables — time (or indenter displacement, h) and the four FRPE material parameters. The range for the FRPE parameters is given in Table 1, and the best-fit material parameters are expected to fall within the chosen range.

(ii) Several values for each parameter are chosen with the upper and lower bounds to generate a 'coarse grid' of material property combinations (Table 1). In the current study, for example, the coarse grid values chosen for E_m were
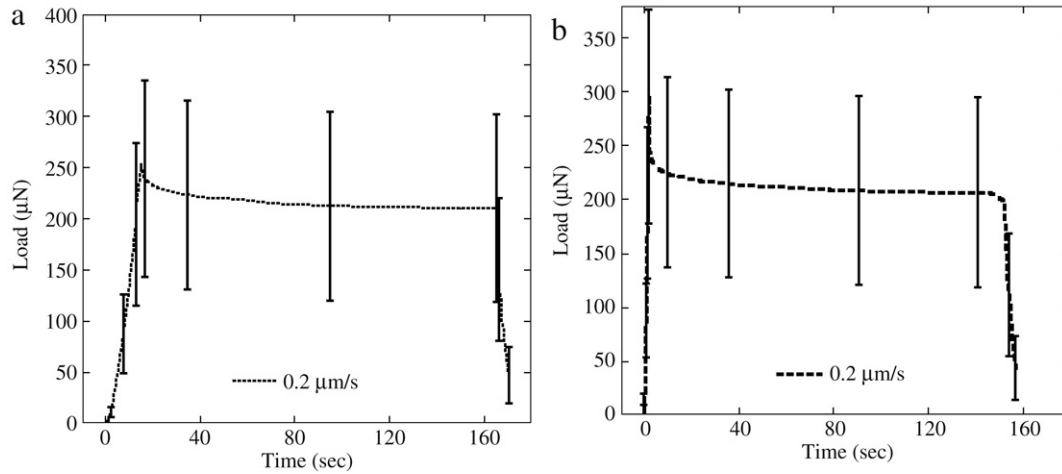
---
[1] Matlab code is available upon request.

Fig. 4 – A typical experimental nanoindentation load response taken at 3.1 μm indentation depth. The response is the average of all 12 indents taken on a single specimen. (a) The loading and initial relaxation response at 0.2 μm/s indentation rate. The total load relaxes by 17.3% within 30 s of the hold time. (b) The loading and initial relaxation at 2 μm/s. The total load relaxes by 29.5% within 20 s of the hold time.

1.0, 1.2, 1.4, . . . , 2.4 MPa. Further, the first material combination in the coarse grid was $(E_m, v_m, \kappa, f_f) = (1.0, 0.05, 0.1, 2.5)$, the second was $(E_m, v_m, \kappa, f_f) = (1.2, 0.05, 0.1, 2.5)$ and so forth until $(E_m, v_m, \kappa, f_f) = (2.4, 0.3, 2, 7.5)$.

(iii) FE solutions for each coarse grid combination are acquired. In the present study, MATLAB was used to call ABAQUS to conduct FE simulations of the nanoindentation experiments. Two simulations were performed for each combination — one at each of the two penetration rates to a maximum penetration depth of 3.1 μm. In the present case, a total of 525 coarse grid combinations exist, and 1050 unique load–displacement curves were generated by the FE simulations.

(iv) A 'fine grid' of material properties is selected; the fine grid includes all the properties from the coarse gird. For example, in the present study, the fine gird values of E_m were 1.0, 1.05, 1.1, 1.15, . . . , 2.4 (Table 1). The first fine grid material property combination was $(E_m, v_m, \kappa, f_f) = (1.0, 0.05, 0.1, 2.5)$, the second was $(E_m, v_m, \kappa, f_f) = (1.05, 0.05, 0.1, 2.5)$, the third was $(E_m, v_m, \kappa, f_f) = (1.1, 0.05, 0.1, 2.5)$ and so forth.

(v) Instead of obtaining the load–displacement (l–d) curves for the additional fine grid material properties via FE simulations, the l–d curves are generated through interpolation between the coarse grid FE solutions. For example, the l–d curves for $(E_m, v_m, \kappa, f_f) = (1.05, 0.05, 0.1, 2.5), (1.1, 0.05, 0.1, 2.5)$, and $(1.15, 0.05, 0.1, 2.5)$ were determined via cubic interpolation between the numerical l–d curves of $(E_m, v_m, \kappa, f_f) = (1.0, 0.05, 0.1, 2.5)$ and $(1.2, 0.05, 0.1, 2.5)$. MATLAB was used for the cubic interpolation in the present work. The interpolation resulted in over 38,000 numerical l–d curves for each displacement rate, and the map of these l–d curves for the all fine grid material properties constituted the interpolant response surface.

Once the IRS was constructed, the best fit material parameters for the nanoindentation curves for each rib were determined by comparing the experimental data from both displacement rates with each of the curves in the IRS using the minimum squared residual. The minimum residual is

the root mean square error between the experimentally measured $(Exp_{s,f})$ and the numerical predicted $(Num_{s,f})$ nanoindentation load response at 3.1 μm defined as:

$$RES = \sum \left(\frac{Exp_s - Num_s}{Exp_s} \right)^2 + \sum \left(\frac{Exp_f - Num_f}{Exp_f} \right)^2 \quad (2)$$

where s and f are the 0.2 μm/s and the 2 μm/s displacement rates, respectively and the summation is taken over all time steps. Simulations with the best-fit parameters from the 3.1 μm response were then used to determine the coefficient of determination (R^2) for the 2.0 μm indentation depth.

5. Results

5.1. Nanoindentation experiments

Safranin-O/Fast Green and Alizarin-Red staining of each of the cartilage specimens confirms that the PCC specimens have a rich, even distribution of proteoglycans and are uncalcified, respectively. Typical nanoindentation load–time curves for both loading rates at the 3.1 μm indentation depth are shown in Fig. 4. For both rates, the indenter load relaxes to within 10% of its equilibrium value within 30 s. As expected, the equilibrium loads (P_{Eq}) for the two rates are within 5%–6% of one another. The differences in P_{Eq} are attributed to small differences (up to 50 nm) in the averaged maximum penetration depth for the two different displacement rates. The maximum penetration depth for indents at 0.2 and 2.0 μm/s at the same position is not always identical because of system drift, which results in drift of the initial tip position during indentation.

For the 3.1 μm indentation depth, the relaxation in the load is 15.8% ± 2.6% and 28.74% ± 2.9% (mean ± S.D.) for the 0.2 μm/s and 2 μm/s displacement rates, respectively and 18.6% ± 3.1% and 32.1% ± 4.3% for the 2.0 μm depth. For all indents, an increase of 20%–22% in the maximum load (P_{max}) is observed with an order of magnitude increase in the indenter displacement rate.

Table 1 – Range of fibril reinforced poroelastic material parameters and coarse and fine material grid combinations. Numerical load–displacement curves for the coarse grid of material property combinations are obtained directly from finite element simulations in ABAQUS. Those for the fine grid combinations are determined via cubic interpolation of the load–displacement curves from the coarse grid in MATLAB.

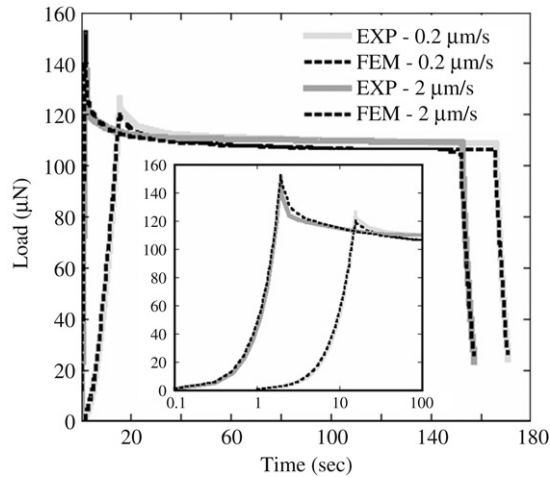| Parameter	Range	Coarse grid values	Fine grid values	Reference
E (MPa)	1.0–2.4	1.0, 1.2, 1.4, 1.6, 1.8, 2.0, 2,4	1.0, 1.05. 1.1, . . . , 2.4	1.8
v	0.05–0.3	0.05, 0.1, 0.15, 0.2, 0.3	0.05, 0.075, 0.01, 0.0125, . . . , 0.3	0.15
$\kappa (10^{-15}) \frac{m^4}{N\,s}$	0.1–2.0	0.1, 0.25, 0.5, 1.2	0.1, 0.15, 0.2, 0.25, . . . , 1, 1.5, 2.0	0.2
f_f (%)	2.5–7.5	2.5, 5.5, 7.5	2.5, 3.5, 4.5, 5.5, 6.5, 7.5	7.5

Fig. 5 – Experimental nanoindentation load data at 3.1 μm indentation depth with numerical curve fits using the best fit fibril reinforced poroelastic model parameters for Specimen 3 at both loading rates. The FRPE simulations are able to predict the load, hold, and unload response for all five cartilage specimens for both indentation depths ($R^2 = 0.988 \pm 0.01$).

5.2.   Fibril reinforced poroelastic model curve fit

Fig. 5 depicts the experimental nanoindentation load data and the corresponding FRPE model curve fits for one of the costal cartilage specimens. Similar results are found for the other specimens, which are not shown. The FRPE model is able to capture the loading, relaxation, and unloading response for both nanoindentation displacement rates simultaneously with a single set of parameters ($R^2 = 0.988 \pm 0.01$). At every point in the curve, the numerical response is within ±10% of the experimental data, though the best fit parameters consistently underestimate the maximum load (P_{max}) for the 0.2 μm/s and overestimate P_{max} for 2 μm/s displacement rates. The range for the best fit FPRE parameters are $E_m = 1.2–2.3$ MPa, $v_m = 0.05–0.15$, $\kappa = 0.05–0.15$, 0.1–0.3 × 10^{-15} m⁴/N s, and $f_f = 5.5–7.5$. The mean ± std for the best-fit material parameters determined from the IRS for all five specimens are $E_m = 1.65 \pm 0.45$ MPa, $v = 0.08 \pm 0.044$, $\kappa = 0.18 \pm 0.09 \times 10^{-15}$ m⁴/N s, and $f_f = 6.7 \pm 0.83$. These parameters are also able to predict the response at 2.0 μm accurately ($R^2 = 0.988 \pm 0.011$).

5.3.   Parametric analysis

Though several authors have elucidated the sensitivity of macroscale simulations of the compression and indentation of cartilage to the different FRPE parameters (Li et al., 1999; Korhonen et al., 2003; Shirazi and Shirazi-Adl, 2005), the sensitivity of the nanoindentation load–displacement response to these parameters remains unknown. A parametric study is now performed to assess the influence of the FRPE properties on the time-dependent and equilibrium nanoindentation response. A reference case with the material properties shown in the last row of Table 1, and an indentation depth of 3.1 μm and rate of 0.2 μm/s, is considered. The reference FRPE properties are representative values within the IRS range, and each parameter is varied so as to underscore the salient characteristics of the model.

The sensitivity of the numerical nanoindentation load response to the different FRPE model parameters is shown in Figs. 6–9. The effects of altering the nonfibrillar matrix properties are depicted in Fig. 6. Both P_{Eq} and P_{max} are nearly proportional to E_m, with a ±45% change in E_m directly resulting in a ±45% and ±39% change in P_{Eq} and P_{max}, respectively. Changes in E_m do not affect the degree of relaxation or the relaxation time, mimicking the trends noted in simulations of bulk experiments. At small values of v_m (<0.2), changes in v_m have a negligible affect on the nanoindentation response. As v_m increases however, both P_{Eq} and P_{max} increase rapidly. Such a rapid rise is expected not only because the nanoindentation load directly increases with increasing v (based simply on Hertz's contact theory) but the increased radial and circumferential strains under the indenter also enhance the nonlinear strain-stiffening effect of the fibers. The extent of relaxation in the material is also diminished as the matrix becomes incompressible due to the decrease in relaxation of the in-plane (radial and circumferential) strains.

Fig. 7 captures the changes in the nanoindentation load response with changes in the permeability. An order of magnitude increase in κ from 0.2 to 2 × 10^{-15} m⁴/N s does not alter P_{Eq} since the pore pressure under the indenter is negligible after the hold period. The greater fluid pressurization results in an increase in P_{max} and an increase in load relaxation time, both of which are more pronounced at the faster displacement rates.

Increasing the volume fraction of fibers (f_f) increases both P_{Eq} and P_{max} (Fig. 8). The percent increase is dependent upon v_m which governs the strain in the fibers and the fraction of the total stress in the solid matrix that they carry. The inclusion of 7.5% fibers only increases the load relaxation
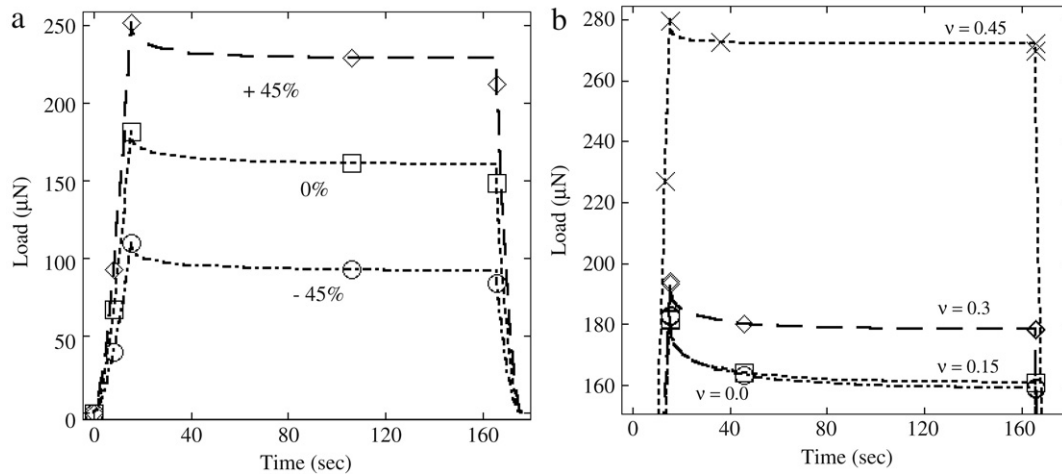
Fig. 6 – **Effect of nonfibrillar matrix properties (a)** E_m **and (b)** v_m **on the simulated nanoindentation load relaxation at 3.1 μm penetration depth at 0.2 μm/s penetration rate. The reference properties are** $E_m = 1.8$ **MPa,** $v_m = 0.15$, $\kappa = 0.2 \times 10^{-15}$ **m^4/N s, and** $f_f = 7.5\%$. **Increasing** E_m **increases both** P_{Eq} **and** P_{max} **without altering the percent relaxation, while increasing** v_m, **particularly for values greater than 0.25, also increases both quantities while decreasing the extent of relaxation.**
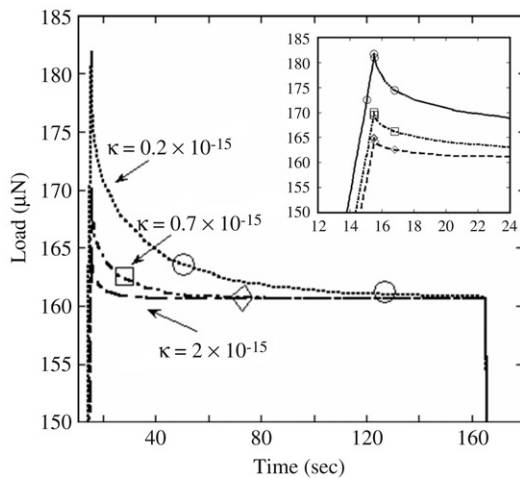

Fig. 7 – **Effects on matrix permeability parameters** κ **on the simulated nanoindentation load response at 3.1 μm penetration depth at 0.2 μm/s penetration rate. The reference properties are** $E_m = 1.8$ **MPa,** $v_m = 0.15$, $\kappa = 0.2 \times 10^{-15}$ **m^4/N s, and** $f_f = 7.5\%$. **While** P_{Eq} **remains constant, increasing** κ **by an order of magnitude sharply decreases** P_{max}, **decreasing the percent relaxation to less than 3%.**

from 8.1% to 11.4% and from 1.1% to 4.0% for $v_m = 0.15$ and $v_m = 0.45$, respectively.

In the present study, 15 different fiber orientations were chosen to represent the distribution of fibers in the PCC network. The orientation of the fibers is crucial to the extent of fiber reinforcement since the orientation determines both whether the fiber is in tension or compression and the extent of strain-stiffening. To determine the effects of orientation on the indenter load, the fiber orientation is altered from 0, ±30° and ±60° to 0, ±20° and ±70° and 0, ±40° and ±50° for the same fiber volume fraction (Fig. 9). Differences within ±3% are observed in P_{Eq} and P_{max} with changes in the fiber orienta-

tion for $v_m = 0.15$. Similar results are seen for $v_m = 0.45$ (data not show). In the elements immediately below the indenter, only rebars oriented in 5 of the 15 directions are under tension. These same 5 fiber directions are active in all three fiber orientations. While the magnitude of the stresses present in the individual fibers changes with changes in orientation, the total fibril stress in an element remains nearly constant (data not shown). Hence, changes to the fibers oriented at ±30° and ±60° has a negligible impact on the load response.

6.   Discussion

The present FRPE model successfully captures the nonlinear nanoindentation behavior of porcine costal cartilage. While the four parameters used in the model are sufficient to describe the time-dependent response at both loading rates, the complexity of the mechanical behavior of orthopaedic soft tissues, especially cartilaginous tissues, requires an accounting of many different constitutive features, including the tension–compression nonlinearity of fibrillar component, the distribution and volume fraction of fibers, the dilation dependent nonlinearity of the permeability, and the intrinsic viscoelasticity of the fiber and nonfibrillar matrix, to comprehensively describe the response in uniaxial tension, in shear, in compression, and indentation (Li et al., 2000; Huang et al., 2003; Wilson et al., 2004; Li et al., 2005; Garcia and Cortes, 2007). Since all facets of the constitutive response cannot be determined from a single set of experiments, the present study also helps to elucidate which parameters may be determined from nanoindentation experiments.

Analogous to the results from unconfined compression and macro-indentation, the equilibrium response (P_{Eq}) in nanoindentation is primarily a function of E_m, v_m, and to a lesser degree, f_f. Since fiber reinforcement increases with increasing indentation depth due to fiber nonlinearity, experiments at different indentation depths and/or with different indenter geometries should allow these parameters
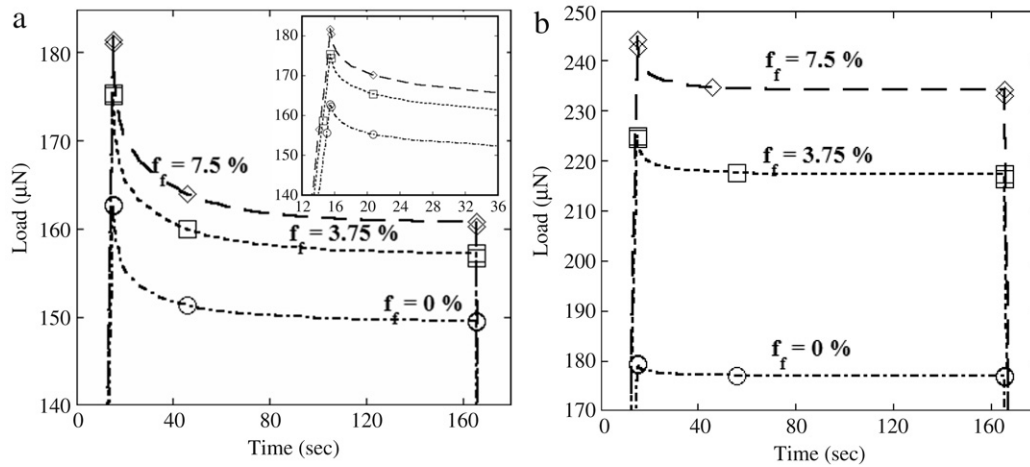
Fig. 8 – Effects on fiber fraction on the simulated nanoindentation load response at 3.1 µm penetration depth at 0.2 µm/s penetration rate at (a) $v_m = 0.15$ and (b) $v_m = 0.45$. The reference properties are $E_m = 1.8$ MPa, $\kappa = 0.2 \times 10^{-15}$ m^4/N s, and $f_f = 7.5\%$. For both values of v_m, increasing f_f increases P_{Eq} and P_{max}, but the results are more prominent for higher v_m.

to be determined uniquely, though an accurate assessment of f_f may only be feasible for materials with higher v_m. According to the simulations, neither fiber orientation nor fiber fraction is an integral factor in the transient response in nanoindentation. This response is in contrast to bulk simulations, where the nonlinear fibers are an integral determinant of the percent load relaxation in the material (Li et al., 1999; Soulhat et al., 1999; Shirazi and Shirazi-Adl, 2005). Not only do the fibers increase the pore pressure by increasing the solid matrix stiffness, for a fixed permeability, the tension–compression nonlinearity enhances the interstitial fluid pressurization at short times, leading to a more much pronounced transient response with a larger fiber fraction (Soltz and Ateshian, 2000). Unlike unconfined compression, where both κ and the nonlinearity permeability parameter M govern the transient response (Li et al., 1999), for nanoindentation both the percent load relaxation and the decay time are governed almost exclusively by κ, especially at small values of v_m. If v_m is known from the equilibrium response, then κ may be determined directly from the transient response in nanoindentation using indents at multiple loading rates.

As indicated by the range and mean ± std of the best-fit FRPE parameters, considerable inter-specimen heterogeity exists between the five PCC specimens. Though the standard deviations in v_m, κ, and f_f are a greater percentage of the mean value than for E_m, the results of the parametric study suggest that the intra- and inter-specimen heterogeneity in the load response is attributed to the differences in the Young's modulus of the nonfibrillar matrix, particularly since the percent load relaxation of all the curves is comparable.

Compared to articular joint cartilage, mechanical characterization of costal cartilage hand has been exceptionally limited. Recent macroscale indentation tests on porcine and human costal cartilage using linear viscoelastic models have reported equilibrium shear moduli in the range of 0.1–2.0 MPa (Mattice et al., 2006; Lau et al., 2008). Assuming a Poisson's ratio of 0.1, similar to the v_m reported here for costal cartilage, the resulting elastic moduli range is from 0.2–4.4 MPa. The
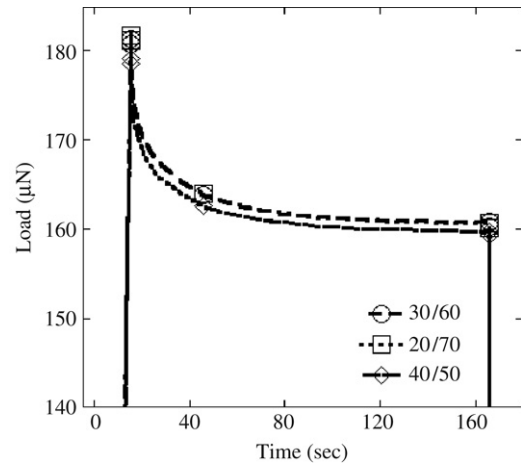

Fig. 9 – Effects on fiber orientation on the simulated nanoindentation load response at 3.1 µm penetration depth at 0.2 µm/s penetration rate at $v_m = 0.15$, with similar results for $v_m = 0.45$. In both cases, the percent load relaxation increases slightly. Changes in fiber orientation are almost indiscernible for lower values of v_m.

equilibrium response of the FRPE model is governed by E_m, and its values here fall within that range. The E_m values found for joint cartilage using FRPE models are lower than those reported here for costal cartilage, ranging from 0.1–0.9 MPa, depending upon site and species (Soulhat et al., 1999; Wilson et al., 2005; Julkunen et al., 2007). These differences may be attributed in part to the higher proteoglycan and collagen fiber content of costal cartilage (Pietila et al., 1999). The fiber volume fraction of articular joint cartilage has been determined to be 3%–4% (Simha et al., 1999; Shirazi and Shirazi-Adl, 2005), while that reported in the present study ranges from 5.5%–7.5%.

To the authors' knowledge, the studies on the permeability of costal cartilage have not been reported. The κ values found in the present study are comparable to those determined by Cao et al. (2006), who utilized a linear poroelastic model to

analyze flat punch nanoindentation tests on mouse articular cartilage. However, these κ values are more than an order of magnitude lower than the 2–8 $\times$ 10^{-15} m^4/N s range commonly cited from bulk experiments on other types of cartilage from many different species, sites, age levels, and constitutive models (Athanasiou et al., 1991, 1994; Li et al., 1999; DiSilvestro et al., 2001).

The κ values predicted by the current model are nearly an order of magnitude lower than those commonly reported. However, increasing κ drastically diminishes the transient response, which all but disappears for κ values in excess of 2×10^{-15} m^4/N s for the slower displacement rate. Since the predicted v_m values are already near zero, the experimentally observed load relaxation of 15.8% $\pm$ 2.6% cannot be achieved with the present model, even with fiber fractions in excess of 20% (not shown). Such κ values would necessitate the inclusion of nonfibrillar matrix viscoelasticity.

The present study ignored the contribution of this intrinsic time dependence of the nonfibrillar matrix, attributing the transient response only to fluid–solid interactions. This exclusion is warranted for several reasons. First, in poroelastic models, the dynamic behavior due to fluid pressurization is determined primarily by the distance between maximum (F_{max}) and zero pore pressure (F_0) boundary condition. For example, in unconfined compression tests, where distance between the F_{max} and the F_0 boundary condition is equal to specimen radius, larger specimens exhibit both longer decay times and high load relaxation magnitudes in comparison to smaller specimens of the same material (Shirazi and Shirazi-Adl, 2005). While the distance between the F_{max} and the F_0 boundary condition scales with experimental length scales, the transience due to the intrinsic viscoelasticity of the nonfibrillar matrix, both in terms of percent load relaxation and relaxation time, should be manifest identically in the nano, micro, and macroscale. In bulk experiments on cartilage, the load relaxation is over 70%, even at moderate strain rates, while in nanoindentation it is less than 30%, even at the high displacement rates. In addition, the relaxation times in macroscale tests are in excess of 100 s, while the transient response in nanoindentation is on the order of 30 s (Lai et al., 1981; DiSilvestro and Suh, 2001; Li and Herzog, 2004b; Lau et al., 2008). Given the difference in length scales, both the extent and the rapidity of the relaxation response in nanoindentation in comparison to bulk experiments suggest that the transience should be dominated by the fluid pressurization. Even if the matrix does possess an intrinsic time dependence, its existence is difficult to confirm from bulk experiments, since its contribution to the relaxation, even at high deformation rates and at short times scales, would be only a very small fraction of the total dynamic response. This may also be the reason why recent fiber reinforced poroviscoelastic models, which incorporate the intrinsic viscoelasticity of the fibers but not the nonfibrillar matrix, have still succeeded in simultaneously describing the results from multiple experiments (Wilson et al., 2004; Li et al., 2005; Garcia and Cortes, 2007).

The present model neglects effects of the electrophysical characteristics of the tissue, such as the fixed charge density and the contribution of osmotic effects to the mechanical nanoindentation response. In the present experiments, these effects should be negligible — the samples are equilibrated in the same PBS bath in which they are immersed prior to and during testing and all tests take place in an enclosed chamber. The change in pH of the PBS solution due to the evaporation of solution is expected to be minimal since there is no measurable difference in the nanoindentation load–displacement curves of indents taken at the same location at the start and the termination of each testing session.

The present study constructed an IRS map to determine a set of best-fit FRPE parameters. The IRS has been used in the past as a method to determine the linear biphasic parameters (E_m, v_m, κ) of articular cartilage from indentation creep experiments (Keenan et al., 2007). While most optimization schemes require thousands of iterations to achieve acceptable convergence and multiple initial starting points to locate a global minimum, the IRS is a simple, gradientless method that automatically searches the entire design space to ensure that a global rather than a local minimum is found. Since the number of simulations required to create a coarse grid of solutions for the IRS scales exponentially with the number of parameters, the IRS is computationally feasible only for material models with five variables or less that have tight upper and lower bounds. Since an IRS must be generated for all unique experiments, optimization methods such as the differential evolution algorithm are more appropriate for simulating results from single, distinct experiments, while the IRS is an efficient scheme when fitting multiple sets of data from identical experiments.

In conclusion, the present work has demonstrated that a fibril reinforced poroelastic model is suitable for describing the time-dependent nanoindentation response of costal cartilage. According to the FE analysis, several facets of the transient response in nanoindentation are unique from those of bulk indentation, but nanoindentation may still be effectively employed to determine both the Young's modulus and the Poisson's ratio of the nonfibrillar solid matrix, the volume fraction of fibers, and the tissue permeability. Experimental studies of soft tissue nanoindentation are presently very limited, but as suitable sample preparations methods, experimental protocols, robust analytical tools and comparisons with traditional bulk experiments are further investigated, nanoindentation has the potential become a ubiquitous tool in the characterization of small, heterogeneous tissues from small animal models. Thus, this work has broad implications for the characterization of soft, nonlinear tissues and provides a method for determining structural properties at constituent length scales.

Acknowledgments

REFERENCES

Athanasiou, K.A., Agarwal, A., et al., 1994. Comparative-study of the intrinsic mechanical-properties of the human acetabular and femoral-head cartilage. Journal of Orthopaedic Research 12 (3), 340–349.

Athanasiou, K.A., Rosenwasser, M.P., et al., 1991. Interspecies comparisons of in situ intrinsic mechanical-properties of distal femoral cartilage. Journal of Orthopaedic Research 9 (3), 330–340.

Balooch, G., Marshall, G.W., et al., 2004. Evaluation of a new modulus mapping technique to investigate microstructural features of human teeth. Journal of Biomechanics 37 (8), 1223–1232.

Bhattacharya, A.K., Nix, W.D., 1988. Finite-element simulation of indentation experiments. International Journal of Solids and Structures 24 (9), 881–891.

Bhushan, B., Williams, V.S., et al., 1988. In situ nanoindentation hardness apparatus for mechanical characterization of extremely thin-films. Journal of Tribology-Transactions of the ASME 110 (3), 563–571.

Bolshakov, A., Oliver, W.C., et al., 1996. Influences of stress on the measurement of mechanical properties using nanoindentation.2. Finite element simulations. Journal of Materials Research 11 (3), 760–768.

Bolshakov, A., Pharr, G.M., 1998. Influences of pileup on the measurement of mechanical properties by load and depth sensing indentation techniques. Journal of Materials Research 13 (4), 1049–1058.

Cao, L., Youn, I., et al., 2006. Compressive properties of mouse articular cartilage determined in a novel micro-indentation test method and biphasic finite element model. Journal of Biomechanical Engineering-Transactions of the ASME 128 (5), 766–771.

Carrillo, F., Gupta, S., et al., 2005. Nanoindentation of poly-dimethylsiloxane elastomers: Effect of crosslinking, work of adhesion, and fluid environment on elastic modulus. Journal of Materials Research 20 (10), 2820–2830.

DiSilvestro, M.R., Suh, J.K.F., 2001. A cross-validation of the biphasic poroviscoelastic model of articular cartilage in unconfined compression, indentation, and confined compression. Journal of Biomechanics 34 (4), 519–525.

DiSilvestro, M.R., Zhu, Q.L., et al., 2001. Biphasic poroviscoelastic simulation of the unconfined compression of articular cartilage: II — Effect of variable strain rates. Journal of Biomechanical Engineering-Transactions of the ASME 123 (2), 198–200.

Doerner, M.F., Nix, W.D., 1986. A method for interpreting the data from depth sensing indentation instruments. Journal of Materials Research 1, 601.

Ebenstein, D.M., Kuo, A., et al., 2004. A nanoindentation technique for functional evaluation of cartilage repair tissue. Journal of Materials Research 19 (1), 273–281.

Ebenstein, D.M., Pruitt, L.A., 2004. Nanoindentation of soft hydrated materials for application to vascular tissues. Journal of Biomedical Materials Research Part A 69A (2), 222–232.

Ebenstein, D.M., Pruitt, L.A., 2006. Nanoindentation of biological materials. Nano Today 1 (3), 26–33.

Elmustafa, A.A., 2007. Pile-up/sink-in of rate-sensitive nanoindentation creeping solids. Modelling and Simulation in Materials Science and Engineering 15 (7), 823–834.

Feng, J.X., Hu, T.Z., et al., 2001. The biomechanical, morphologic, and histochemical properties of the costal cartilages in children with pectus excavatum. Journal of Pediatric Surgery 36 (12), 1770–1776.

Fortin, M., Soulhat, J., et al., 2000. Unconfined compression of articular cartilage: Nonlinear behavior and comparison with a fibril-reinforced biphasic model. Journal of Biomechanical Engineering-Transactions of the ASME 122 (2), 189–195.

Franke, O., Durst, K., et al., 2007. Mechanical properties of hyaline and repair cartilage studied by nanoindentation. Acta Biomaterialia 3 (6), 873–881.

Garcia, J.J., Cortes, D.H., 2007. A biphasic viscohyperelastic fibril-reinforced model for articular cartilage: Formulation and comparison with experimental data. Journal of Biomechanics 40 (8), 1737–1744.

Gupta, S., Carrillo, F., et al., 2005. Simulated soft tissue nanoindentation: A finite element study. Journal of Materials Research 20 (8), 1979–1994.

Haque, F., 2003. Application of nanoindentation to development of biomedical materials. Surface Engineering 19 (4), 255–268.

Haut, R.C., Little, R.W., 1972. A constitutive equation of collagen fibers. Journal of Biomechanics 5 (5), 423–430.

Hertz, H., 1881. Ueber die Beruhrung Fester Elastischer Korper. Journal für die Reine und Angewandte Mathematik 92, 156.

Ho, S.P., Balooch, M., et al., 2004. Ultrastructure and nanomechanical properties of cementum dentin junction. Journal of Biomedical Materials Research Part A 68A (2), 343–351.

Hu, K., Radhakrishnan, P., et al., 2001. Regional structural and viscoelastic properties of fibrocartilage upon dynamic nanoindentation of the articular condyle. Journal of Structural Biology 136 (1), 46–52.

Huang, C.Y., Soltz, M.A., et al., 2003. Experimental verification of the roles of intrinsic matrix viscoelasticity and tension–compression nonlinearity in the biphasic response of cartilage. Journal of Biomechanical Engineering-Transactions of the ASME 125 (1), 84–93.

Julkunen, P., Kiviranta, P., et al., 2007. Characterization of articular cartilage by combining microscopic analysis with a fibril-reinforced finite-element model. Journal of Biomechanics 40 (8), 1862–1870.

Keenan, K.E., Kourtis, L., et al. 2007. Web-based Resource for the Computation of Cartilage Biphasic Material Properties with the Interpolant Response Surface Method. Transactions of the Orthopaedic Research Society, San Diego, CA.

Korhonen, R.K., Laasanen, M.S., et al., 2003. Fibril reinforced poroelastic model predicts specifically mechanical behavior of normal, proteoglycan depleted and collagen degraded articular cartilage. Journal of Biomechanics 36 (9), 1373–1379.

Lai, W.M., Mow, V.C., 1980. Drag-induced compression of articular-cartilage during a permeation experiment. Biorheology 17 (1–2), 111–123.

Lai, W.M., Mow, V.C., et al., 1981. Effects of non-linear strain-dependent permeability and rate of compression on the stress behavior of articular-cartilage. Journal of Biomechanical Engineering-Transactions of the ASME 103 (2), 61–66.

Lau, A., Oyen, M.L., et al., 2008. Indentation stiffness of aging human costal cartilage. Acta Biomaterialia 4, 97–103.

Lei, F.L., Szeri, A.Z., 2007. Inverse analysis of constitutive models: Biological soft tissues. Journal of Biomechanics 40 (4), 936–940.

Leong, P.L., Morgan, E.F., 2008. Measurement of fracture callus material properties via nanoindentation. Acta Biomaterialia.

Li, C., Pruitt, L.A., et al., 2006. Nanoindentation differentiates tissue-scale functional properties of native articular cartilage. Journal of Biomedical Materials Research Part A 78A (4), 729–738.

Li, L.P., Buschmann, M.D., et al., 2000. A fibril reinforced nonhomogeneous poroelastic model for articular cartilage: Inhomogeneous response in unconfined compression. Journal of Biomechanics 33 (12), 1533–1541.

Li, L.P., Buschmann, M.D., et al., 2001. The asymmetry of transient response in compression versus release for cartilage in unconfined compression. Journal of Biomechanical Engineering-Transactions of the ASME 123 (5), 519–522.

Li, L.P., Herzog, W., 2004a. The role of viscoelasticity of collagen fibers in articular cartilage: Theory and numerical formulation. Biorheology 41 (3–4), 181–194.

Li, L.P., Herzog, W., 2004b. Strain-rate dependence of cartilage stiffness in unconfined compression: The role of fibril reinforcement versus tissue volume change in fluid pressurization. Journal of Biomechanics 37 (3), 375–382.

Li, L.P., Herzog, W., et al., 2005. The role of viscoelasticity of collagen fibers in articular cartilage: Axial tension versus compression. Medical Engineering & Physics 27 (1), 51–57.

Li, L.P., Soulhat, J., et al., 1999. Nonlinear analysis of cartilage in unconfined ramp compression using a fibril reinforced poroelastic model. Clinical Biomechanics 14 (9), 673–682.

Li, X.D., An, Y.H.H., et al., 2007. Microindentation test for assessing the mechanical properties of cartilaginous tissues. Journal of Biomedical Materials Research Part B-Applied Biomaterials 80B (1), 25–31.

Mak, A.F., Lai, W.M., et al., 1987. Biphasic indentation of articular-cartilage. 1. Theoretical-analysis. Journal of Biomechanics 20 (7), 703–714.

Mallinger, R., Stockinger, L., 1988. Amianthoid (asbestoid) transformation — electron microscopical studies on aging human costal cartilage. American Journal of Anatomy 181 (1), 23–32.

Mattice, J.M., Lau, A.G., et al., 2006. Spherical indentation load-relaxation of soft biological tissues. Journal of Materials Research 21 (8), 2003–2010.

Morgan, F.R., 1960. Mechanical properties of collagen and leather fibres. American Leather Chemical Assoc Journal 55 (1), 23–24.

Olberding, J.E., Suh, J.K.F., 2006. A dual optimization method for the material parameter identification of a biphasic poroviscoelastic hydrogel: Potential application to hypercompliant soft tissues. Journal of Biomechanics 39 (13), 2468–2475.

Oliver, W.C., Pharr, G.M., 1992. An improved technique for determining hardness and elastic modulus using load and displacement sensing indentation experiments. Journal of Materials Research 7 (6), 1564–1583.

Oyen, M.L., 2006. Analytical techniques for indentation of viscoelastic materials. Philosophical Magazine 86 (33–35), 5625–5641.

Oyen, M.L., 2008. Poroelastic nanoindentation responses of hydrated bone. Journal of Materials Research 23 (5), 1307–1314.

Oyen, M.L., Ko, C.C., 2007. Examination of local variations in viscous, elastic, and plastic indentation responses in healing bone. Journal of Materials Science-Materials in Medicine 18 (4), 623–628.

Pharr, G.M., Oliver, W.C., 1992. Measurement of thin-film mechanical-properties using nanoindentation. MRS Bulletin 17 (7), 28–33.

Pietila, K., Kantomaa, T., et al., 1999. Comparison of amounts and properties of collagen and proteoglycans in condylar, costal and nasal cartilages. Cells Tissues Organs 164 (1), 30–36.

Rho, J.Y., Roy, M.E., et al., 1999. Elastic properties of microstructural components of human bone tissue as measured by nanoindentation. Journal of Biomedical Materials Research 45 (1), 48–54.

Sakai, M., 2002. Time-dependent viscoelastic relation between load and penetration for an axisymmetric indenter. Philosophical Magazine a-Physics of Condensed Matter Structure Defects and Mechanical Properties 82 (10), 1841–1849.

Shirazi, R., Shirazi-Adl, A., 2005. Analysis of articular cartilage as a composite using nonlinear membrane elements for collagen fibrils. Medical Engineering & Physics 27 (10), 827–835.

Simha, N.K., Fedewa, M., et al., 1999. A composites theory predicts the dependence of stiffness of cartilage culture tissues on collagen volume fraction. Journal of Biomechanics 32 (5), 503–509.

Sneddon, I.N., 1965. The relation between load and penetration in the axisymmetric Boussinesq problem for a punch of arbitrary profile. International Journal of Engineering Science 3 (1), 47–57.

Soltz, M.A., Ateshian, G.A., 2000. A conewise linear elasticity mixture model for the analysis of tension–compression nonlinearity in articular cartilage. Journal of Biomechanical Engineering-Transactions of the ASME 122 (6), 576–586.

Soulhat, J., Buschmann, M.D., et al., 1999. A fibril-network-reinforced biphasic model of cartilage in unconfined compression. Journal of Biomechanical Engineering-Transactions of the ASME 121 (3), 340–347.

Warner, M.D., Taylor, W.R., et al., 2001a. Finite element biphasic indentation of cartilage: A comparison of experimental indenter and physiological contact geometries. Proceedings of the Institution of Mechanical Engineers Part H-Journal of Engineering in Medicine 215 (H5), 487–496.

Warner, M.D., Taylor, W.R., et al., 2001b. A method for determining contact between a non-porous surface and articular cartilage in a biphasic FE model. In: Middleton, J., Jones, M.L., Pande, G. (Eds.), Computer Methods in Biomechanics and Bioengineering - 3. Gordon and Breach Science Publishers, pp. 207–212.

Weppelmann, E., Swain, M.V., 1996. Investigation of the stresses and stress intensity factors responsible for fracture of thin protective films during ultra-micro indentation tests with spherical indenters. Thin Solid Films 286 (1–2), 111–121.

Wilson, W., van Donkelaar, C.C., et al., 2004. Stresses in the local collagen network of articular cartilage: A poroviscoelastic fibril-reinforced finite element study. Journal of Biomechanics 37 (3), 357–366.

Wilson, W., van Donkelaar, C.C., et al., 2005. A fibril-reinforced poroviscoelastic swelling model for articular cartilage. Journal of Biomechanics 38 (6), 1195–1204.

Zysset, P.K., Guo, X.E., et al., 1999. Elastic modulus and hardness of cortical and trabecular bone lamellae measured by nanoindentation in the human femur. Journal of Biomechanics 32 (10), 1005–1012.

Selected reviewer comments and author responses for this paper

Reviewer: Why did the authors choose to study costal cartilage vs knee joint articular cartilage?

Authors: Though studies on articular joint cartilage are abundant, joint cartilage possesses both inplane and depth-dependent inhomogeneity (superficial zone vs middle zone vs deep zone). Further, the orientation of the collagen fibers in the superficial and deep zones imparts an anisotropy to these layers. All of these factors further complicate the construction of the FRPE finite element model, requiring the thickness of each layer to be determined and the creation of transition zones of fiber orientation. The primary reason for choosing the costal cartilage was related to the uniformity of the composition cartilage over the test volumes and the random distribution of collagen fibers in the matrix. Though the middle zone of joint cartilage also possesses these attributes, the authors onlyhad access to freshly slaughtered porcine

tissue, in which knee joint cartilage is only a few mm thick. Microtoming away superficial and deep zones proved difficult to do precisely. A further aim of the study, not reported here, was the comparison of FRPE results obtained from nanoindentation with unconfined compression tests. Such a comparison is feasible only with an isotropic material.

Reviewer: Pg. 7, point of contact determination, how was the contact point determined "visually"? This is imprecise, many metrics use a certain change in load or stiffness, or take a derivative of the curve to find the transition, or many other options. Just looking at the plot and stating "well I think that's about the first point" is potentially fraught with error.

Authors: As described in the response to Comment #16 by Reviewer 3, the total tip displacement was adjusted for every position to ensure that the maximum indentation (or penetration) depth was either 2.0 or 3.1 µm. The initial point-of-contact had to be determined while the tests were in progress, which hindered the authors' ability to use a metric requiring an external software program (for example a custom written MATLAB program). Further, any curve that deviated from the 2.0 or 3.1 µm maximum penetration depth by more than ±50–55 µm was discarded and immediately retaken (after another 3 min recovery). A "visual" inspection of the curves was conducted during the experiments as follows:

Immediately after each curve was taken, the authors viewed the load–displacement curve with the TriboIndenter software, zooming in where the initial change in the load appeared. Since the indents were commenced from above the sample surface, the initial stiffness of the curve was zero (or nearly zero). For every curve, a distinct change in stiffness could be observed as the indenter came into contact with the cartilage. The load at the point of the stiffness change was noted (it wasn't always zero due to system drift), and the initial point of contact was assumed to occur after a change in load of 0.25 µN. None of these procedures could be effectively "standardized" and were thus conducted visually by the experimenters as tests were in progress. However, an error in the initial displacement of ±35–40 nm would lead to an error in the load of less than 5% in any individual curve. Given the scatter in the individual curves and the variability across a single sample, the authors believe that these differences do not significantly impact the ability of the FRPE model to predict either the nanoindentation response of the costal cartilage or the values of the FRPE parameters.

Reviewer: Some mention of the uniqueness of the solution is given, however, a map of the search space might be nice to see if other parameter sets approached the local minimum.

Authors: Since the search space is five-dimensional (the four fibril reinforced poroelastic material parameters and time), its physical map cannot be displayed in three dimensions. Thus, it is not possible to visualize the search space. However, to assess whether or not other parameter sets approached the constrained minimum, the authors also had the MATLAB program sort the residuals of the interpolant response surface from lowest to highest and report the parameters sets for which the residuals were lowest (1st), and then 100th, 200th, 300th, and 400th in the ranking. For all 5 specimens, the parameter sets with the 100–500 rankings only differed from the minimum parameter set by a small change in either one or two parameters. For example, for Specimen 2, the parameter set with the lowest residual was $(E_m, v_m, \kappa, f_f) = (1.75, 0.05, 0.25, 7.5)$ while the parameter set with the 400th lowest residual was $(E_m, v_m, \kappa, f_f) = (1.75, 0.20, 0.2, 7.5)$.